NASA TM X-53634

AEROELASTIC LOAD GROWTH EFFECTS ON SATURN CONFIGURATIONS

By James G. Papadopoulos
Aero-Astrodynamics Laboratory

NASA

*George C. Marshall
Space Flight Center,
Huntsville, Alabama*

AEROELASTIC LOAD GROWTH EFFECTS ON SATURN CONFIGURATIONS

By

James G. Papadopoulos

George C. Marshall Space Flight Center

Huntsville, Alabama

ABSTRACT

The effects of aerodynamic loads induced by static aeroelasticity are analyzed for the Saturn configurations. This aeroelastic load growth is shown, for any given Mach number, to increase at an accelerated rate with increases in dynamic pressure. During the period of high dynamic pressure, the Saturn control requirements due to aeroelastic effects are significant. The unexplained external body moments recorded during the Saturn I Block II flights are correlated to aeroelastic load growth. Local aerodynamic bending moments are increased at a time in flight when the vehicle loadings are already large and near design limits. This aeroelastic load growth is additional to that of flexible bending mode dynamics and should be included when analyzing wind profiles for vehicle loadings.

NASA - GEORGE C. MARSHALL SPACE FLIGHT CENTER

NASA - GEORGE C. MARSHALL SPACE FLIGHT CENTER

Technical Memorandum X-53634

July 14, 1967

AEROELASTIC LOAD GROWTH EFFECTS ON SATURN CONFIGURATIONS

by

James G. Papadopoulos

DEFINITION OF SYMBOLS

Symbol	Definition
$A, B, C, \ldots, I$	curve fit angle-of-attack distribution coefficients representing the aeroelastic load growth
$a_j, b_j, \ldots, i_j$	elastic curve-fit coefficients corresponding to an equilibrium angle-of-attack distribution of $\alpha = \eta^j$.
$a_I, b_I, \ldots, i_I$	elastic curve-fit coefficients corresponding to the static angular deflection of initial loading
CP/D	rigid body center of pressure, calibers from station 100
$\Delta CP/D$	aeroelastic load growth center of pressure, calibers from station 100
CG/D	vehicle center of gravity, calibers from station 100
C_{N_α}	rigid normal force coefficient gradient, per degree
ΔC_{N_α}	incremental normal force coefficient gradient due to aeroelastic load growth, per degree
$(C_{N_\alpha})_{FLEX}$	flexible normal force coefficient gradient (sum of rigid and aeroelastic), per degree
C_1	aerodynamic moment coefficient about c.g., $(rad/sec^2)(1/rad)$
D	vehicle reference diameter, meters
$M_{AEROELASTIC}$	aerodynamic moment about vehicle's center of gravity due to the aeroelastic load growth, N-M
N'/M	aerodynamic force coefficient, $(m/sec^2)(1/rad)$
q	free stream dynamic pressure, N/M^2
S	vehicle reference area, M^2
α_I	initial angle-of-attack distribution over vehicle, radians

DEFINITIONS OF SYMBOLS (Continued)

Symbol	Definition
α_E	elastic angle-of-attack distribution over vehicle, radians
α_F	final angle-of-attack distribution over vehicle, radians
η	nondimensional vehicle station, where $\eta = 0$ at gimbal station

Superscripts

$'$	elastic curve-fit coefficients based on a unit value of dynamic pressure, q

LIST OF ILLUSTRATIONS

TECHNICAL MEMORANDUM X-53634

AEROELASTIC LOAD GROWTH EFFECTS ON SATURN CONFIGURATIONS

SUMMARY

The static aeroelastic effect on aerodynamic loadings was deter-
mined for the Saturn configurations. The results indicate an appre-
ciable increase in the vehicle bending loads. For the Saturn V
configuration, vehicle station 3100 inches, a critical stage splice,
had a 26 percent increase in shears and bending moments due to static
aeroelasticity at a flight condition of 12 degrees angle-of-attack at
Mach 1.2. This 26 percent increase is composed of 19 percent due to
static deflections and 7 percent due to iterative aerodynamic load
growth. The net aeroelastic load growth varies along the vehicle
length and, consequently, causes changes in the total center of pres-
sure which alter the vehicle's stability.

The nonlinearity of aeroelasticity with aerodynamic lift distri-
butions and dynamic pressure precludes any readily available numerical
factor by which this effect can be superficially included. In general,
as the vehicle flight loads are increased, the aeroelastic effect also
increases. Saturn flight tests have already indicated many discrep-
ancies in aerodynamic data. This flight test error, hitherto labeled as
an unknown external aerodynamic moment, is attributed to static
aeroelasticity.

I. INTRODUCTION

The effect of elastic vehicles on flight loads has, in the past,
been limited to the analysis of bending mode feedback through the closed
loop control sensors. While such an approach includes vehicle bending
mode dynamics, there is no provision for determining the aerodynamic
load growth induced by vehicle flexibility. This report presents an
analytical evaluation of the aerodynamic load growth or steady state
aeroelastic effect for Saturn configurations.

Aeroelastic considerations are a particularly important factor in
determining the steady state flight loads of a vehicle because, in a
flight environment, the vehicle's deflected shape causes changes in
local angle of attack. These changes in local angle of attack will
induce an additional aerodynamic loading causing further increases in
local angles of attack. The resultant deflected shape is an equili-
brium between local aerodynamic forces and vehicle stiffness.

A noniterative superposition method of aeroelastic analysis is presented in this report. Although the analytic evaluation was based on quasi-steady aerodynamics, the nonlinear aerodynamic characteristics of the lift gradient were included in the analysis.

II. ANALYSIS

The steady state aeroelastic effects on flight loads are evaluated from the angle-of-attack distribution at which equilibrium is established. The mathematical approach presented here is based on a noniterative superposition technique which is now described.

The following angle-of-attack symbols are used:

α_I = initial angle-of-attack distribution

α_E = elastic angle-of-attack distribution

α_F = final angle-of-attack distribution at which equilibrium is established.

Their relationship is defined as

$$\alpha_F = \alpha_I + \alpha_E. \tag{1}$$

The problem is to determine the elastic angle-of-attack distribution for any given flight condition. For the Saturn vehicle, the elastic angle-of-attack distribution can be sufficiently represented by an eighth order polynomial of vehicle station. Letting η be the nondimensional vehicle station, where $\eta = 0$ at the gimbal station and $\eta = 1.0$ at the nose, then

$$\alpha_E = A + B\eta + C\eta^2 + D\eta^3 + E\eta^4 + F\eta^5 + G\eta^6 + H\eta^7 + I\eta^8. \tag{2}$$

To develop this aeroelastic solution, it is necessary to digress at this point and contemplate known solutions. For example, if the equilibrium angle-of-attack distributions were known, then the elastic angle-of-attack distribution could readily be computed as static angular deflections from the vehicle's structural properties and the known loadings. The results can then be curve-fitted, in this instance, to an eighth order η polynomial. Therefore, if

$$\alpha_{Fj} = \eta^j \tag{3}$$

2

where j = 0, 1, ..., 8, then, the curve-fitted polynomial coefficients can be computed for each elastic angle-of-attack distribution.

$$\alpha_{Ej} = a_j + b_j\eta + c_j\eta^2 + d_j\eta^3 + e_j\eta^4 + f_j\eta^5 + g_j\eta^6 + h_j\eta^7 + i_j\eta^8. \quad (4)$$

For the general aeroelastic solution, the initial angle-of-attack distribution due to the static deflection can be computed and represented as an eighth degree η polynomial:

$$\alpha_I = a_I + b_I\eta + c_I\eta^2 + d_I\eta^3 + e_I\eta^4 + f_I\eta^5 + g_I\eta^6 + h_I\eta^7 + i_I\eta^8. \quad (5)$$

Now substituting equation (2) into equation (1), we obtain

$$\alpha_F = \alpha_I + A + B\eta + C\eta^2 + D\eta^3 + E\eta^4 + F\eta^5 + G\eta^6 + H\eta^7 + I\eta^8 \quad (6)$$

and, by using the definitions of equation (3),

$$\alpha_F = \alpha_I + A\alpha_{F0} + B\alpha_{F1} + C\alpha_{F2} + D\alpha_{F3} + E\alpha_{F4} + F\alpha_{F5} + G\alpha_{F6} + H\alpha_{F7} + I\alpha_{F8}. \quad (7)$$

Now, writing the initial angle-of-attack distributions for each term in equation (7) yields

$$\alpha_I = \alpha_I - (a_I + b_I\eta + c_I\eta^2 + d_I\eta^3 + e_I\eta^4 + f_I\eta^5 + g_I\eta^6 + h_I\eta^7 + i_I\eta^8)$$
$$+ B\alpha_{I1} + C\alpha_{I2} + D\alpha_{I3} + E\alpha_{I4} + F\alpha_{I5} + G\alpha_{I6} + H\alpha_{I7} + I\alpha_{I8}, \quad (8)$$

which will reduce to

$$A\alpha_{I0} + B\alpha_{I1} + C\alpha_{I2} + \ldots + I\alpha_{I8} = a_I + b_I\eta + c_I\eta^2 + \ldots + i_I\eta^8. \quad (9)$$

3

Now the initial angle-of-attack distribution of each term on the left-hand side of equation (9) can be written as the final angle of attack minus the elastic angle-of-attack distribution.

$$A[(1 - a_0) - b_0\eta - c_0\eta^2 - \ldots - i_0\eta^8] + B[-a_1 + (1 - b_1)\,\eta - c_1\eta^2$$

$$- \ldots - i_1\eta^8] + C[-a_2 - b_2\eta + (1 - c_2)\,\eta^2 - \ldots - i_2\eta^8]$$

$$+ \ldots + I[-a_8 - b_8\eta - c_8\eta^2 - \ldots + (1 - i_8)\eta^8]$$

$$= \alpha_I + b_I\eta + c_I\eta^2 + d_I\eta^3 + e_I\eta^4 + f_I\eta^5 + g_I\eta^6 + h_I\eta^7 + g_I\eta^8. \quad (10)$$

By equating power coefficients of η, the coefficients of the elastic angle-of-attack distribution can be determined from the following equation:

$$
\begin{bmatrix}
(1-a_0) & -a_1 & -a_2 & -a_3 & -a_4 & -a_5 & -a_6 & -a_7 & -a_8 \\
-b_0 & (1-b_1) & -b_2 & -b_3 & -b_4 & -b_5 & -b_6 & -b_7 & -b_8 \\
-c_0 & -c_1 & (1-c_2) & -c_3 & -c_4 & -c_5 & -c_6 & -c_7 & -c_8 \\
-d_0 & -d_1 & -d_2 & (1-d_3) & -d_4 & -d_5 & -d_6 & -d_7 & -d_8 \\
-e_0 & -e_1 & -e_2 & -e_3 & (1-e_4) & -e_5 & -e_6 & -e_7 & -e_8 \\
-f_0 & -f_1 & -f_2 & -f_3 & -f_4 & (1-f_5) & -f_6 & -f_7 & -f_8 \\
-g_0 & -g_1 & -g_2 & -g_3 & -g_4 & -g_5 & (1-g_6) & -g_7 & -g_8 \\
-h_0 & -h_1 & -h_2 & -h_3 & -h_4 & -h_5 & -h_6 & (1-h_7) & -h_8 \\
-i_0 & -i_1 & -i_2 & -i_3 & -i_4 & -i_5 & -i_6 & -i_7 & (1-i_8)
\end{bmatrix}
\begin{Bmatrix} A \\ B \\ C \\ D \\ E \\ F \\ G \\ H \\ I \end{Bmatrix}
=
\begin{Bmatrix} a_I \\ b_I \\ c_I \\ d_I \\ e_I \\ f_I \\ g_I \\ h_I \\ i_I \end{Bmatrix}.
$$

(11)

It can be seen that the basic equation for the aeroelastic coefficients, equation (11), bears much similarity to the characteristics equations for vehicle bending dynamics. There are, in fact, many more subtle similarities, including divergent vehicle velocity, which is analogous to a natural frequency in bending dynamics. This nonlinearity with dynamic pressure is more evident by defining a set of prime coefficients which represent the deflected curve fits based on a unit value of dynamic pressure.

Then

$$a_n = a'_n q$$

$$\vdots \qquad \vdots$$

$$i_n = i'_n q \tag{12}$$

where n = 0,1,2, ..., 8, and I. Now, dividing both sides of equation (11)
by q results in the following set of characteristic equations:

$$
\begin{bmatrix}
\left(\tfrac{1}{q} - a'_0\right) & -a'_1 & -a'_2 & -a'_3 & -a'_4 & -a'_5 & -a'_6 & -a'_7 & -a'_8 \\
-b'_0 & \left(\tfrac{1}{q} - b'_1\right) & -b'_2 & -b'_3 & -b'_4 & -b'_5 & -b'_6 & -b'_7 & -b'_8 \\
-c'_0 & -c'_1 & \left(\tfrac{1}{q} - c'_2\right) & -c'_3 & -c'_4 & -c'_5 & -c'_6 & -c'_7 & -c'_8 \\
-d'_0 & -d'_1 & -d'_2 & \left(\tfrac{1}{q} - d'_3\right) & -d'_4 & -d'_5 & -d'_6 & -d'_7 & -d'_8 \\
-e'_0 & -e'_1 & -e'_2 & -e'_3 & \left(\tfrac{1}{q} - e'_4\right) & -e'_5 & -e'_6 & -e'_7 & -e'_8 \\
-f'_0 & -f'_1 & -f'_2 & -f'_3 & -f'_4 & \left(\tfrac{1}{q} - f'_5\right) & -f'_6 & -f'_7 & -f'_8 \\
-g'_0 & -g'_1 & -g'_2 & -g'_3 & -g'_4 & -g'_5 & \left(\tfrac{1}{q} - g'_6\right) & -g'_7 & -g'_8 \\
-h'_0 & -h'_1 & -h'_2 & -h'_3 & -h'_4 & -h'_5 & -h'_6 & \left(\tfrac{1}{q} - h'_7\right) & -h'_8 \\
-i'_0 & -i'_1 & -i'_2 & -i'_3 & -i'_4 & -i'_5 & -i'_6 & -i'_7 & \left(\tfrac{1}{q} - i'_8\right)
\end{bmatrix}
\begin{Bmatrix} A \\ B \\ C \\ D \\ E \\ F \\ G \\ H \\ I \end{Bmatrix}
=
\begin{Bmatrix} a'_I \\ b'_I \\ c'_I \\ d'_I \\ e'_I \\ f'_I \\ g'_I \\ h'_I \\ i'_I \end{Bmatrix}
\tag{13}
$$

This technique can be extended to include the aeroelastic fin twist
effect (see reference 1).

III. RESULTS

A. Aeroelastic Effect on Saturn I Block II and Comparison with Flight Tests

The aeroelastic load growth characteristics of the Saturn I Block II vehicles were determined for various Mach number and dynamic pressure combinations. Quasi-steady state aerodynamics was assumed, and the aerodynamic loadings for the various angle-of-attack distributions [2], as defined by equation (3), were computed by multiplying the local lift gradient with the local angle-of-attack distribution. The coefficients of the final angle-of-attack distribution (A $\rightarrow$ I, equation (11)) were evaluated, and the aerodynamic loading on the vehicle determined using superposition techniques.

Since the equilibrium loadings are referenced to that of a unit angle of attack at the gimbal station, the vehicle's deflected shape increases the lift coefficient and moves the center of pressure forward of that predicted by theoretical aerodynamics for an undeflected vehicle. In figure 2, the increase in lift coefficient gradient, ΔC_{N_α}, is seen to be dependent on both Mach number and dynamic pressure. This is not too surprising since the aeroelastic characteristic equations (equation (11)) are nonlinear with dynamic pressure. The center-of-pressure location of this lift gradient is indicated as $\Delta CP/D$ in terms of calibers forward of the gimbal station (figure 3). The aerodynamic moment about the vehicle's center of gravity due to this aeroelastic load growth is

$$M_{aeroelastic} = (\Delta C_{N_\alpha}) \left(\frac{\Delta CP}{D} - \frac{CG}{D}\right) \alpha qSD. \tag{14}$$

Flight tests results of Saturn I Block II vehicles confirm the analytical calculations of the aeroelastic load growth. The flight instrumentation of these vehicles included both Q-Ball and fin-mounted angle-of-attack meters. With no aeroelastic load growth considered, flight test correlation between the angle-of-attack meters and the gimbal engine deflections required an external applied moment. This unexplained moment, which was described as aerodynamic in nature, was observed to be relatively large in pitch and yaw. The peak values of these unexplained external moments, as recorded in the MSFC Flight Test Evaluation Reports [3,4,5,6], are shown in the last column of Table I. Using the flight conditions at the time of the peak external moments, the aerodynamic moments due to the aeroelastic load growth were computed from equation (14). Comparisons between the observed flight test unexplained external moment and the moment due to aeroelasticity indicate good agreement in magnitude and direction for all flights in both pitch and yaw. Thus, inclusion of the aeroelastic load growth would have greatly reduced or eliminated the unexplained external moments from reconstructed flight simulations.

6

TABLE I

Comparison of Aeroelastic Moment With Observed Flight Test External Moment

Saturn Flight Vehicle	Time (sec)	α (deg)	Mach	q	ΔC_N	$\frac{\Delta CP}{D}$	Moment Due to Aero- elasticity (N-M)	Observed[*] Flight Test Unexplained External Moment (N-M)
SA-7, Pitch	76.5	1.47	1.93	36,000	.0134	5.12	376,000	700,000
SA-7, Yaw	72.0	1.4	1.70	36,500	.0128	4.88	430,000	430,000
SA-8, Pitch	64.0	1.42	1.3	33,500	.0095	4.53	268,000	650,000
SA-8, Yaw	72.7	0.8	1.85	31,800	.0115	5.02	205,000	270,000
SA-9, Pitch	63.5	1.47	1.46	33,200	.0105	4.64	316,000	650,000
SA-9, Yaw	69.0	1.5	1.63	33,100	.0109	4.77	349,000	270,000
SA-10, Pitch	75.0	.95	1.85	32,000	.0115	5.05	247,000	500,000
SA-10, Yaw	75.6	1.0	1.77	32,300	.0112	4.96	246,000	200,000

[*]References 3,4,5, and 6.

Present six-degrees-of-freedom trajectory simulation programs can be readily converted to include the aeroelastic load growth effect. The procedure would require utilizing the flexible aeroelastic coefficients from the following equations:

$$(C_{N\alpha})_{flex} = (C_{N\alpha}) + (\Delta C_{N\alpha})_{aeroelastic} \qquad (15)$$

$$(CP/D)_{flex} = \frac{(C_{N\alpha})(CP/D) + (\Delta C_{N\alpha})(\Delta CP/D)_{aeroelastic}}{C_{N\alpha} + (\Delta C_{N\alpha})_{aeroelastic}} . \qquad (16)$$

Since $(\Delta C_{N_\alpha})_{aeroelastic}$ is a function of both Mach number and dynamic pressure, the final flexible lift gradient and center-of-pressure coefficients must be evaluated for each specific flight trajectory. Possibly the best scheme would be to incorporate equations (15) and (16) within the program and use a look-up table as part of the input for $(\Delta C_{N_\alpha})_{aeroelastic}$ and $(\Delta CP/D)_{aeroelastic}$ (figures 2 and 3).

B. Local Bending Moment Effect on Saturn IB

The static aeroelastic effect on local aerodynamic bending moments was investigated for the Saturn IB configuration (figure 4). The percentage of increase of the induced aeroelastic bending moment component to the rigid body aerodynamic bending moment was plotted as a function of vehicle station for various Mach numbers with a fin angle of attack of one degree and dynamic pressure equal to 20,000 and 30,000 N/M^2 in figures 5 and 6, respectively. The aeroelastic effects increase slightly from the gimbal station toward the nose. For q = 20,000 N/M^2, the aeroelastic increase is between 7 and 14 percent, while for q = 30,000 N/M^2, the aeroelastic increase is between 11 and 22 percent.

To determine the aeroelastic nonlinearity with angle of attack, a particular vehicle station (station 1663 inches) was analyzed for various angles of attack and dynamic pressures at Mach 1.0 and Mach 1.2 [7]. The results shown in figures 7 and 8 indicate the nonlinearity angle-of-attack effect to be significantly more important at Mach 1.0 than Mach 1.2. Also, for any given condition, the percentage of local aerodynamic bending moment will increase with dynamic pressure.

C. Local Bending Moment Effect on Saturn V

An aeroelastic analysis was made for Saturn V using linear aerodynamics in the low angle-of-attack region ($\alpha < 2°$). Figure 9 summarizes the percentage of increase of the local aerodynamic bending moment at station 3100 inches resulting from aeroelastic load growth. At increasing values of dynamic pressure, the aeroelastic component increases in significance. These percentages of increase in local aerodynamic bending moment of Saturn V are reasonably similar to those of Saturn IB equivalent vehicle station 1540 inches (figures 5 and 6).

Using the dynamic pressure profile consistent with the standard 502 flight trajectory, the aeroelastic load growth was computed using nonlinear aerodynamics at various angles of attack for Mach numbers 0.9, 1.0, and 1.2 [8]. The resulting increases in aerodynamic bending moments at vehicle station 3100 are shown in figure 10. A load condition of 12 degrees angle of attack at Mach 1.2 will induce approximately 26 percent increase in the aerodynamic bending moment. Nineteen percent

8

of this 26 percent aeroelastic increase in bending moment is due to static deflections and 7 percent is due to iterative aerodynamic load growth.

The aeroelastic effects on the Saturn V normal aerodynamic force coefficients and aerodynamic moment coefficients were evaluated at Mach 1.2 (figures 11 and 12) and at Mach 1.7 (figures 13 and 14). For comparisons, these total vehicle coefficients were computed (1) for a rigid vehicle (shown as solid lines), (2) for a flexible vehicle bend under original loading (shown as dashed lines), and (3) for a flexible vehicle whose deflected shape results from considering both bending and iterative load growth, or total aeroelastic effect (shown as dotted lines). Examination of these total vehicle aerodynamic coefficients indicates that the total aeroelastic effect is significant with respect to the bending effect particularly at large dynamic pressures and large angles of attack. At Mach 1.2 with a dynamic pressure of 30,000 N/M^2 and a 12-degree angle of attack, bending effects increase rigid body aerodynamics by 9 percent in normal force coefficient and 35 percent in the total aerodynamic moment coefficient. Analysis of the same condition, using the total aeroelastic effect, which includes both bending and iterative load growth, results in increases to rigid body aerodynamics amounting to 12 percent in normal force coefficient and 43 percent in total aerodynamic moment coefficient. Similar comparisons are indicated at Mach 1.7 in figures 13 and 14.

The bending and total aeroelastic evaluations for the aerodynamic normal force and moment coefficients shown in figures 11 through 14 were obtained using an eighth order polynomial curve fit solution for the vehicle's deflected distribution. A similar approach could, in fact, be obtained from equation (11) using generalized bending mode coordinates. Since these coordinates are a convenient means of introducing vehicle bending dynamics into trajectory control studies, their use in evaluating aeroelastic characteristics was investigated. The aerodynamic coefficients resulting from changes in local angle of attack due to bending and static aeroelasticity were computed using an eighth degree polynomial and compared with results using as many as the first four bending modes. In addition, an exact solution of these aerodynamic coefficients was obtained from actual angular deflection resulting from the initial loading and the final equilibrium loading. The results of this comparison (see table II) indicate that considerably more than four bending modes are required to approach the accuracy of an eighth order polynomial. Furthermore, by comparing the bending column of bending mode approximations to the total aeroelastic value of the exact solution, yet neglecting the iterative aeroelastic load growth, the effect of including bending modes can be evaluated. For this particular flight condition, including only bending effects as approximated by the first bending mode will result in underestimating N'/M by 8 percent and C_1 by

12 percent. If the first four bending modes were included, then this error would be reduced to underestimating N'/M by 7 percent and C_1 by 8 percent.

Table II

Comparisons of Aeroelastic Coefficients Resulting From A
Polynomial Curve Fit Versus Bending Mode

	N'/M	M/sec^2	$1/rad$	C_1	$\dfrac{rad}{sec^2}$	$1/rad$
	Rigid	Bending	Total Aeroelastic	Rigid	Bending	Total Aeroelastic
Exact Solution	6.72	7.36	7.52	-0.174	-0.233	-0.247
8th Order Polynomial	6.72	7.36	7.52	-0.174	-0.234	-0.249
1st Bending Mode	6.72	6.92	6.94	-0.174	-0.214	-0.219
1st and 2nd Bending Modes	6.72	6.94	6.96	-0.174	-0.228	-0.234
1st, 2nd, & 3rd Bending Modes	6.72	6.97	6.98	-0.174	-0.228	-0.234
1st, 2nd, 3rd, & 4th Bending Modes	6.72	7.00	7.01	-0.174	-0.229	-0.235
Saturn V Flight Conditions: Mach = 1.2 $\alpha = 12°$ q = 30,000 N/M^2						

IV. CONCLUSIONS AND RECOMMENDATIONS

The Saturn aeroelastic effects are significantly important during the period of maximum dynamic pressure. At this period the induced aerodynamic loading decreases the vehicle's stability and increases the component of local aerodynamic bending moment. The large external

body moments recorded as unexplained during Saturn I Block II flight tests result from changes in aerodynamic load distributions induced by aeroelasticity.

It is recommended that six-degrees-of-freedom simulation programs, such as prelaunch wind monitorship, be modified to include the Saturn aeroelastic loadings. Such a program modification could be readily incorporated by storing the precomputed aeroelastic loads as a function of Mach number, dynamic pressure, and angle of attack. While this represents an appreciable amount of information, it would need to be computed only once for any geometric and stiffness configuration of the Saturn vehicle. An alternate approach would be to precompute the aeroelastic effects for specific trajectories and alter this input for significant changes in flight trajectories.

An investigation of the downwash effects, which were neglected in this report, is recommended. This would require modifying the aerodynamic loadings for the various elastic angle-of-attack distributions and using these loadings to determine the aeroelastic superposition solution. The investigation would be greatly enhanced by wind tunnel tests of Saturn models with known rigid deflected shapes.
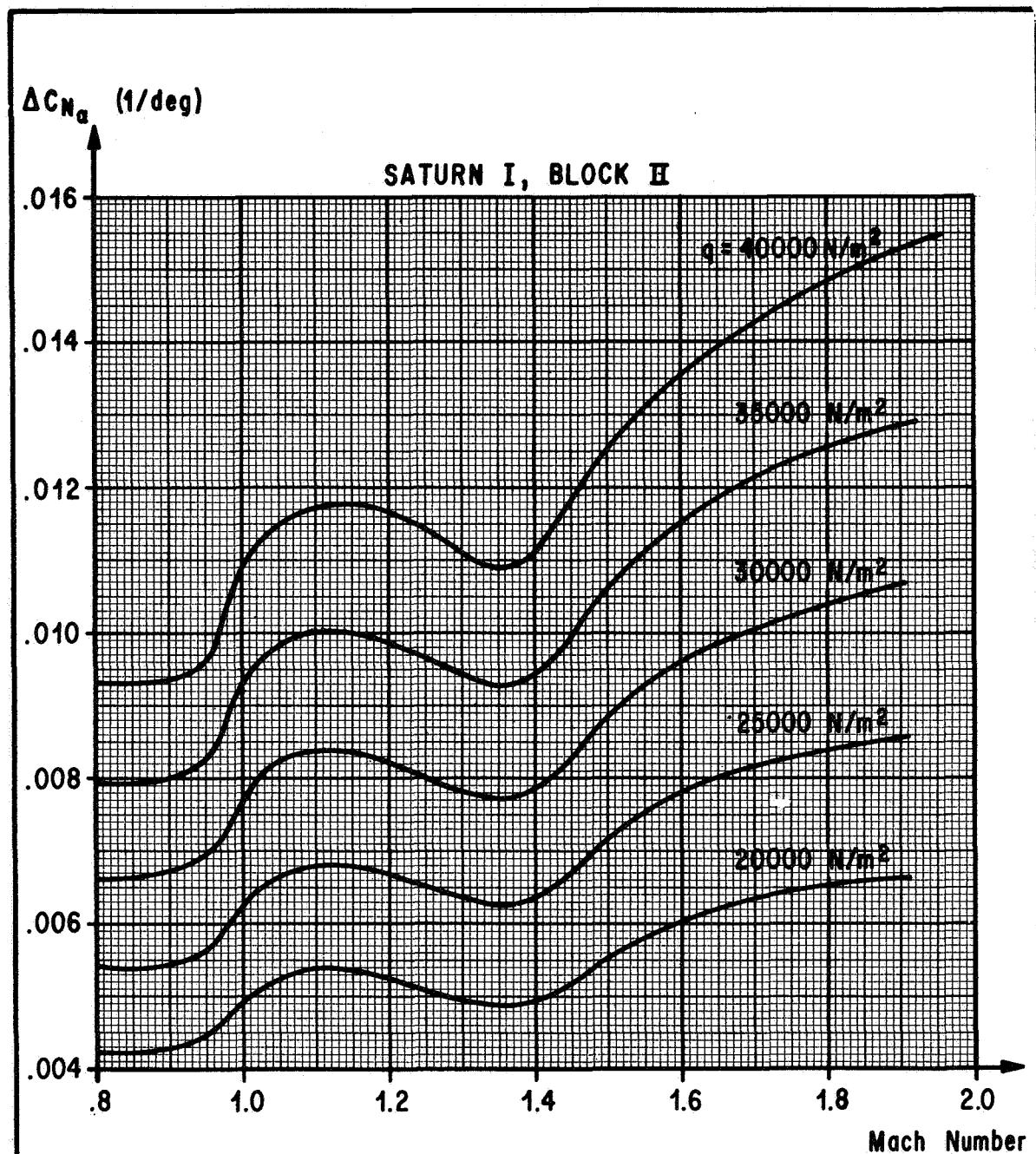
$$(C_{N_\alpha})_{Flex} = C_{N_\alpha} + \Delta C_{N_\alpha}$$
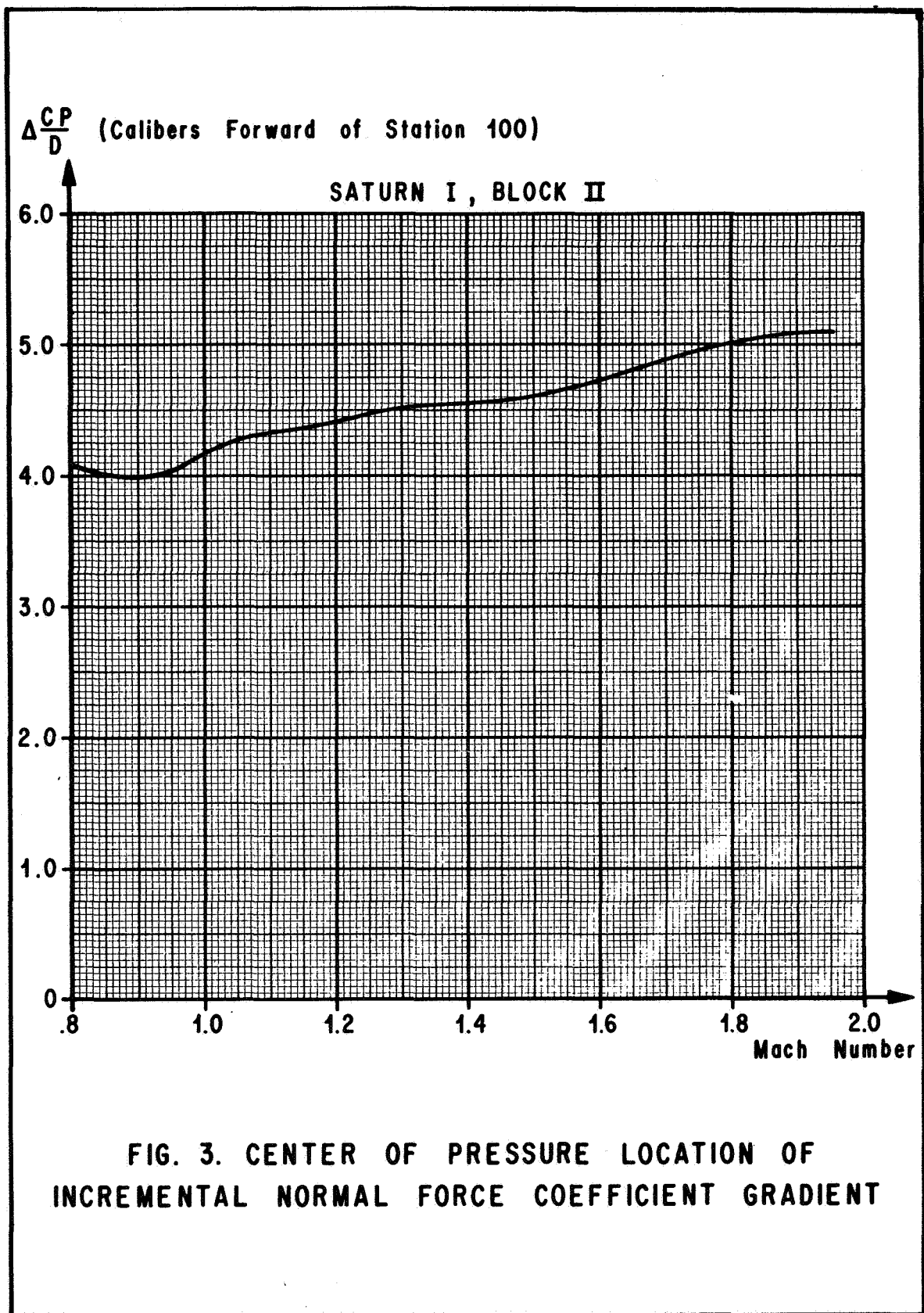
Where : C_{N_α} is Rigid Vehicle Aerodynamics.

ΔC_{N_α} is Induced Aerolastic Load Growth

ΔC_{N_α}

C_{N_α}

$\Delta CP/D$

CP/D

CG/D

Gimbal Sta 100.0
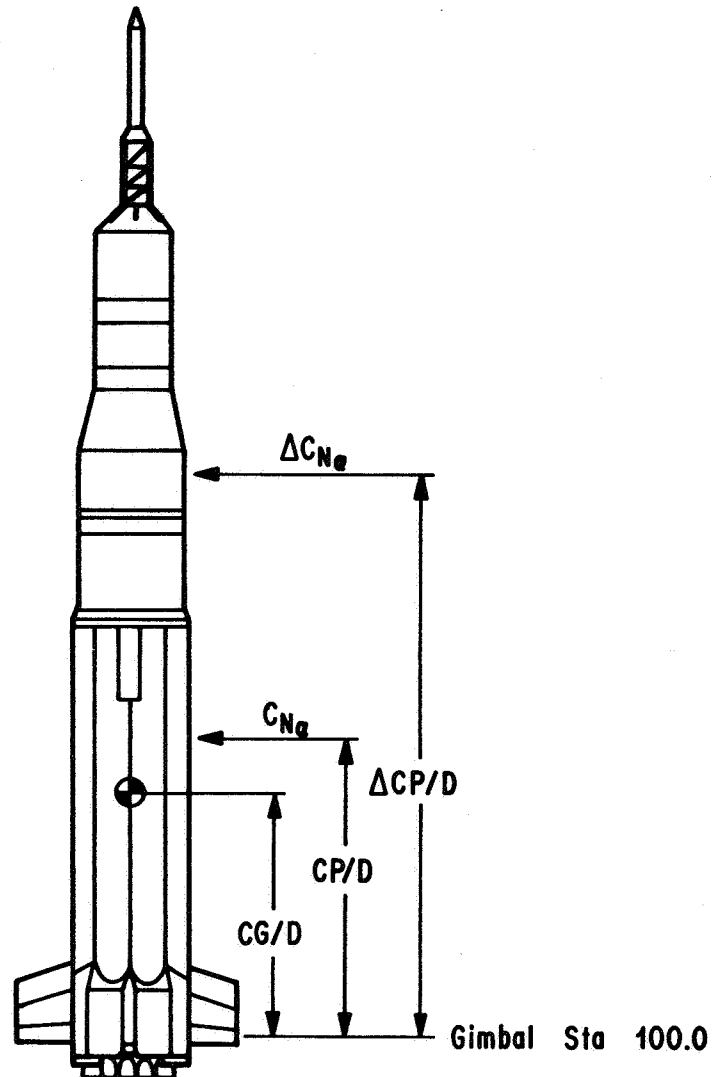
FIG. 1. RIGID AND INDUCED
AEROELASTIC NORMAL FORCE COEFFICIENT GRADIENTS

FIG. 2. INCREASE IN NORMAL FORCE COEFFICIENT
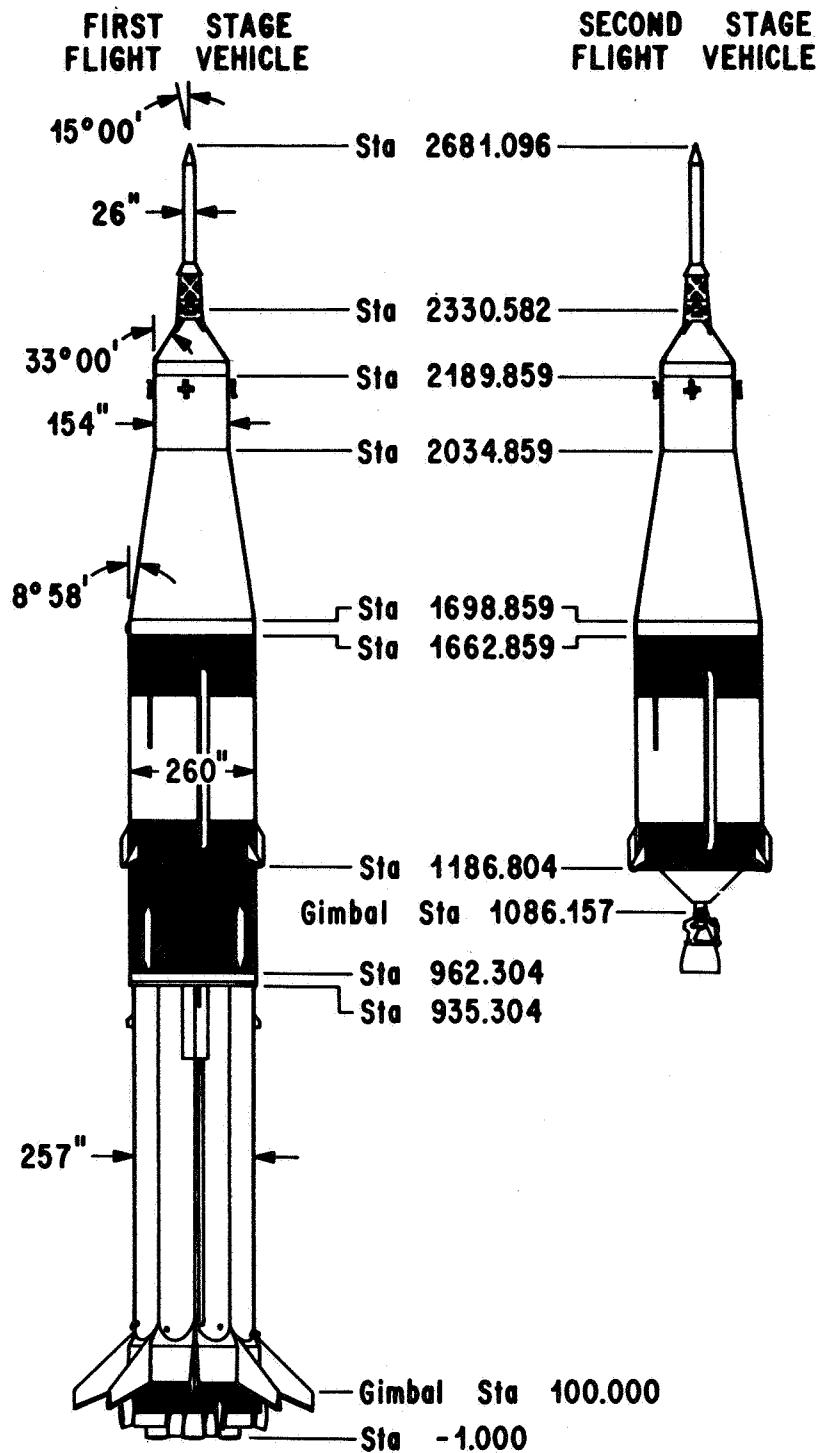GRADIENT DUE TO AEROELASTIC LOAD GROWTH

FIG. 3. CENTER OF PRESSURE LOCATION OF
INCREMENTAL NORMAL FORCE COEFFICIENT GRADIENT

FIRST STAGE
FLIGHT VEHICLE

SECOND STAGE
FLIGHT VEHICLE

15°00'

26"

Sta 2681.096

Sta 2330.582

33°00'

Sta 2189.859

154"

Sta 2034.859

8°58'

Sta 1698.859
Sta 1662.859

260"

Sta 1186.804

Gimbal Sta 1086.157

Sta 962.304
Sta 935.304

257"

Gimbal Sta 100.000
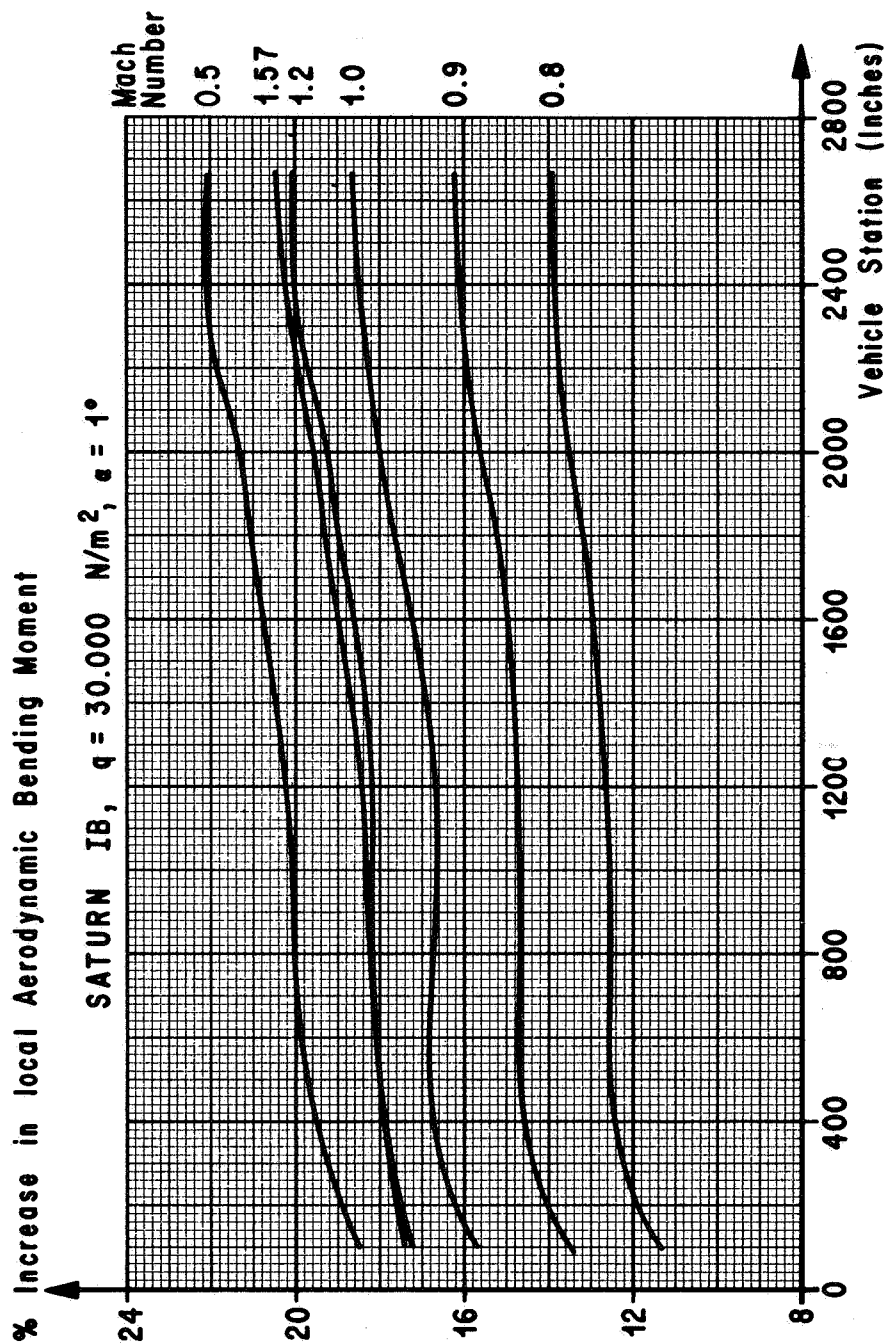
Sta -1.000

FIG. 4. GEOMETRY OF
THE APOLLO - SATURN FLIGHT VEHICLE

15
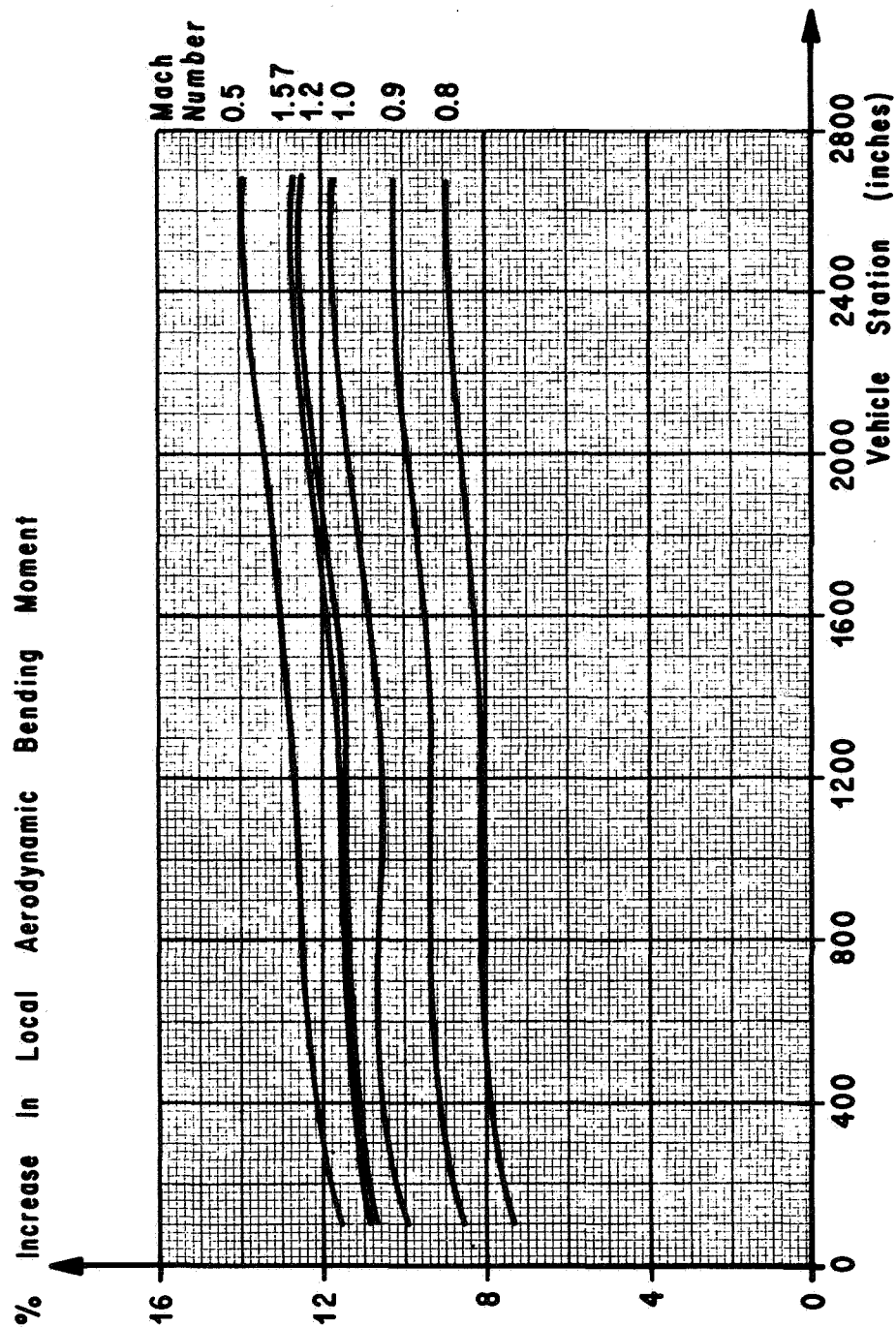
FIG. 5. INCREASE IN LOCAL AERODYNAMIC BENDING MOMENT DUE TO AEROELASTIC LOAD GROWTH FOR SATURN IB AT q = 20,000 N/m²

% Increase in local Aerodynamic Bending Moment
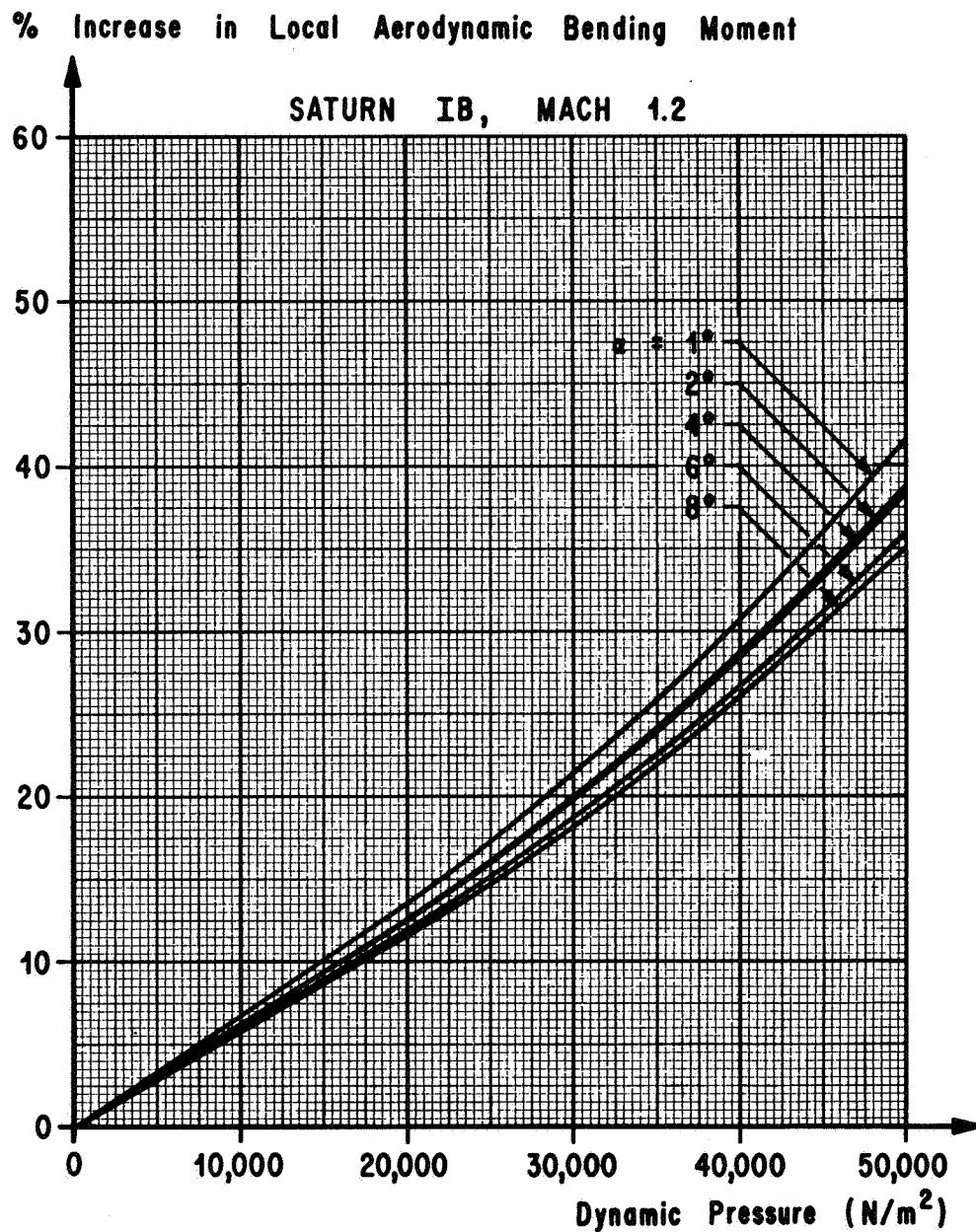
SATURN IB, q = 30.000 N/m², α = 1°

Mach Number

0.5
1.57
1.2
1.0
0.9
0.8

Vehicle Station (Inches)

FIG. 6. INCREASE IN LOCAL AERODYNAMIC BENDING MOMENT DUE TO AEROELASTIC LOAD GROWTH FOR SATURN IB AT q = 30,000 N/m²
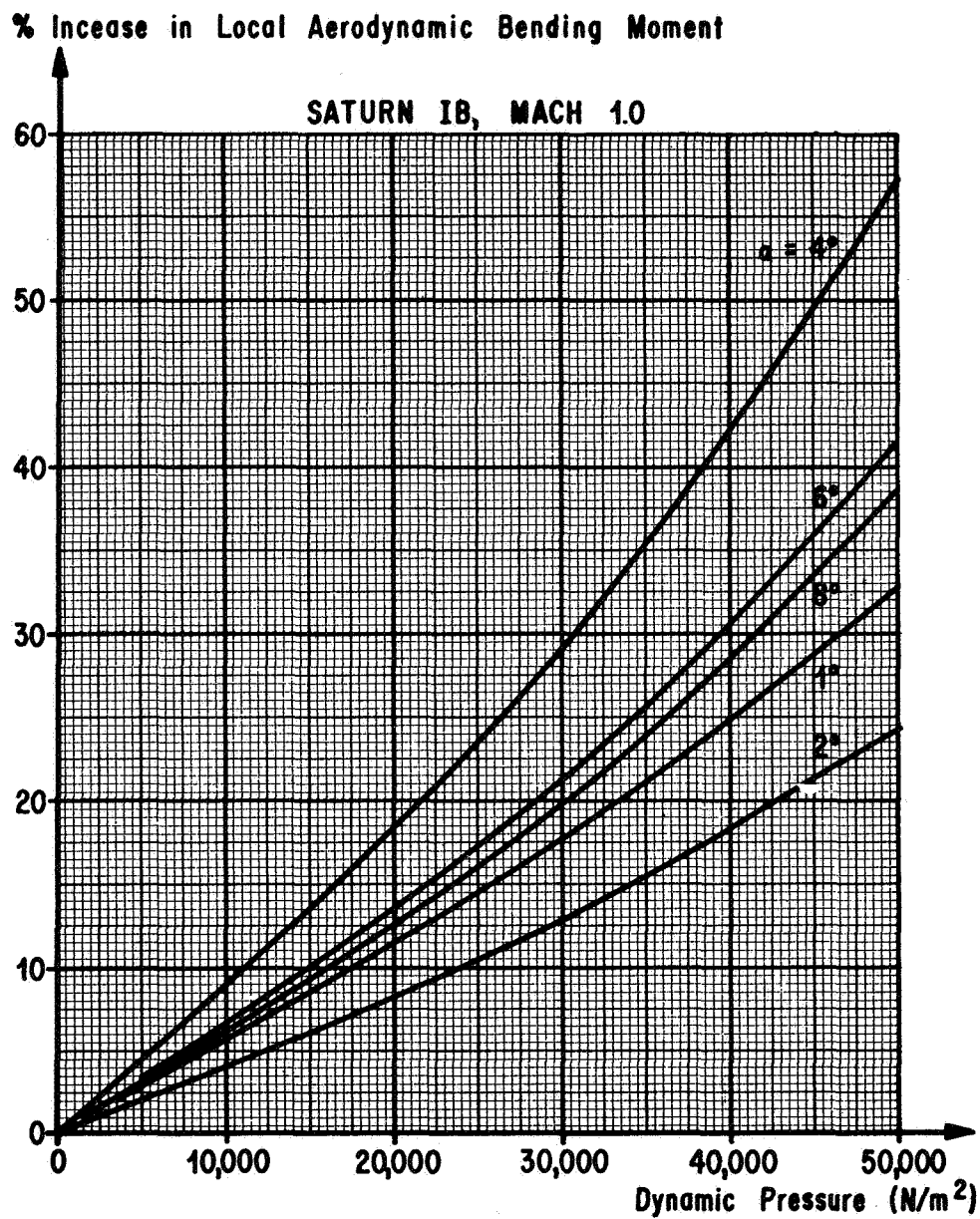
% Incease in Local Aerodynamic Bending Moment

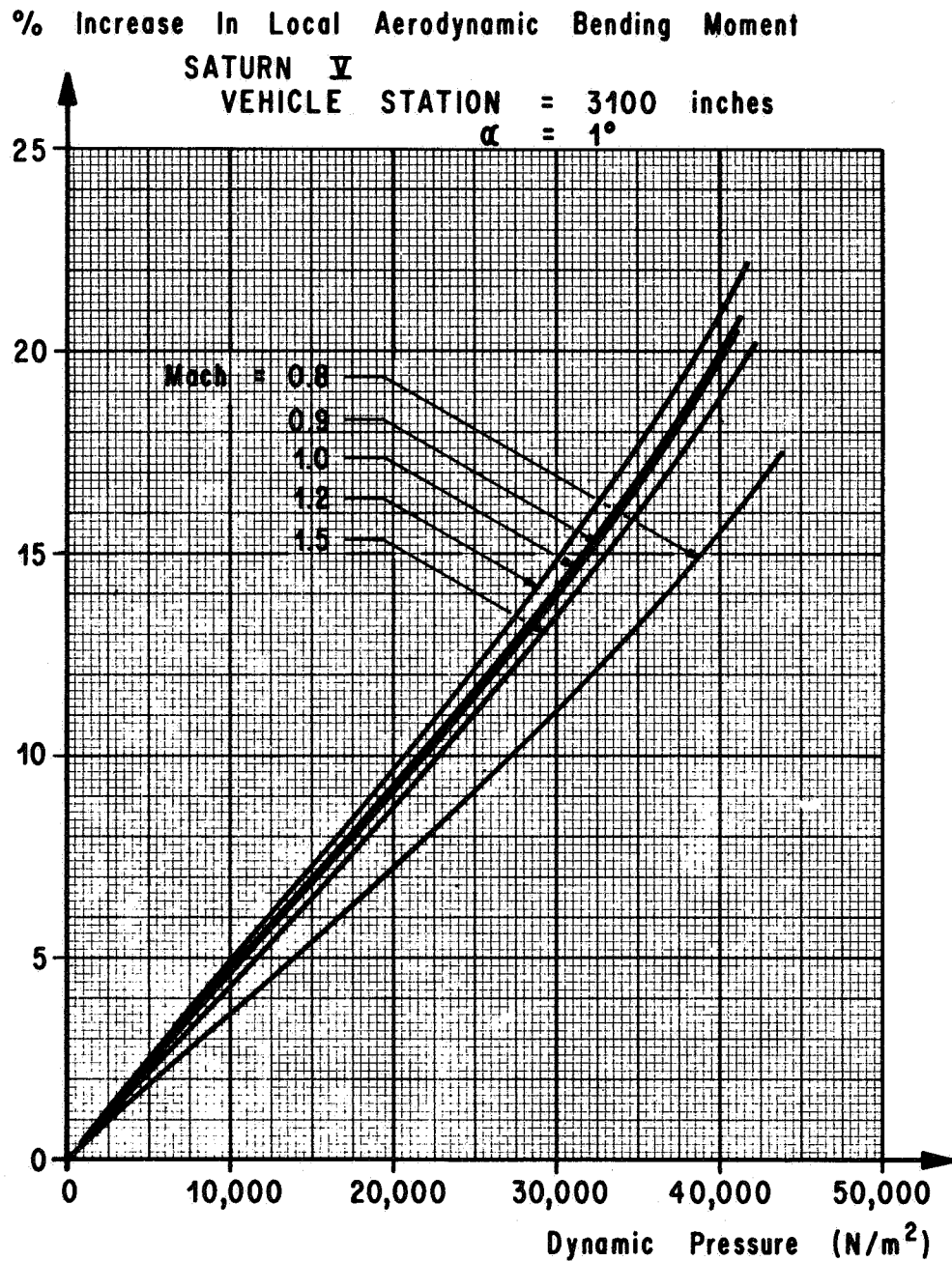SATURN IB, MACH 1.0

$\alpha = 10°$

8°

6°

4°

2°

Dynamic Pressure (N/m^2)

FIG. 7. EFFECT OF NONLINEAR ANGLE OF ATTACK
AERODYNAMICS ON AEROELASTIC BENDING MOMENT
AT STATION 1663 INCHES FOR MACH 1.0

% Increase in Local Aerodynamic Bending Moment

SATURN IB, MACH 1.2

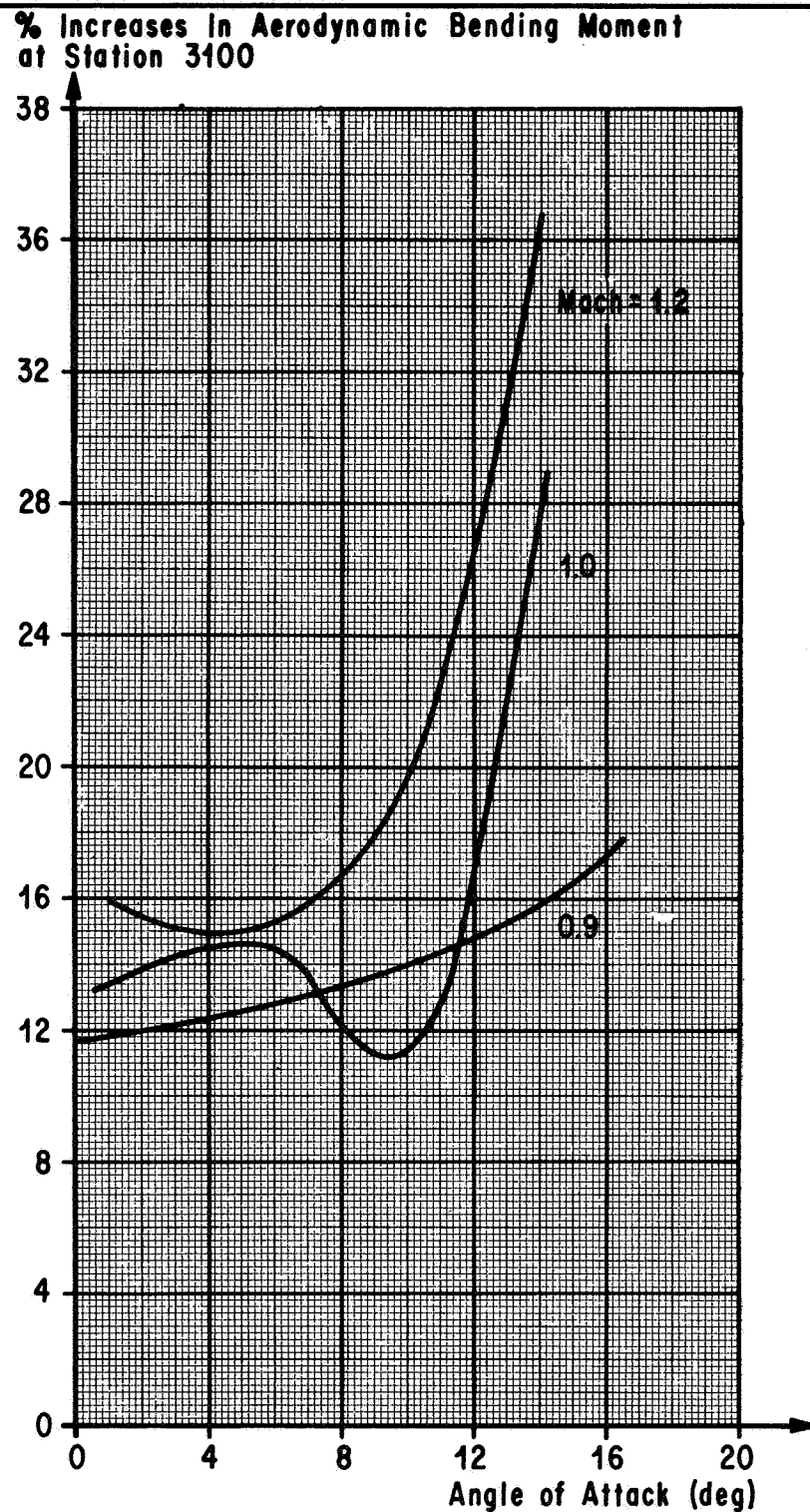

FIG. 8. EFFECT OF NONLINEAR ANGLE OF ATTACK
AERODYNAMICS ON AEROELASTIC BENDING MOMENT
AT STATION 1663 INCHES FOR MACH 1.2

FIG. 9. INCREASE IN LOCAL AERODYNAMIC BENDING MOMENT DUE TO AEROELASTIC LOAD GROWTH FOR SATURN V AT STATION 3100 INCHES

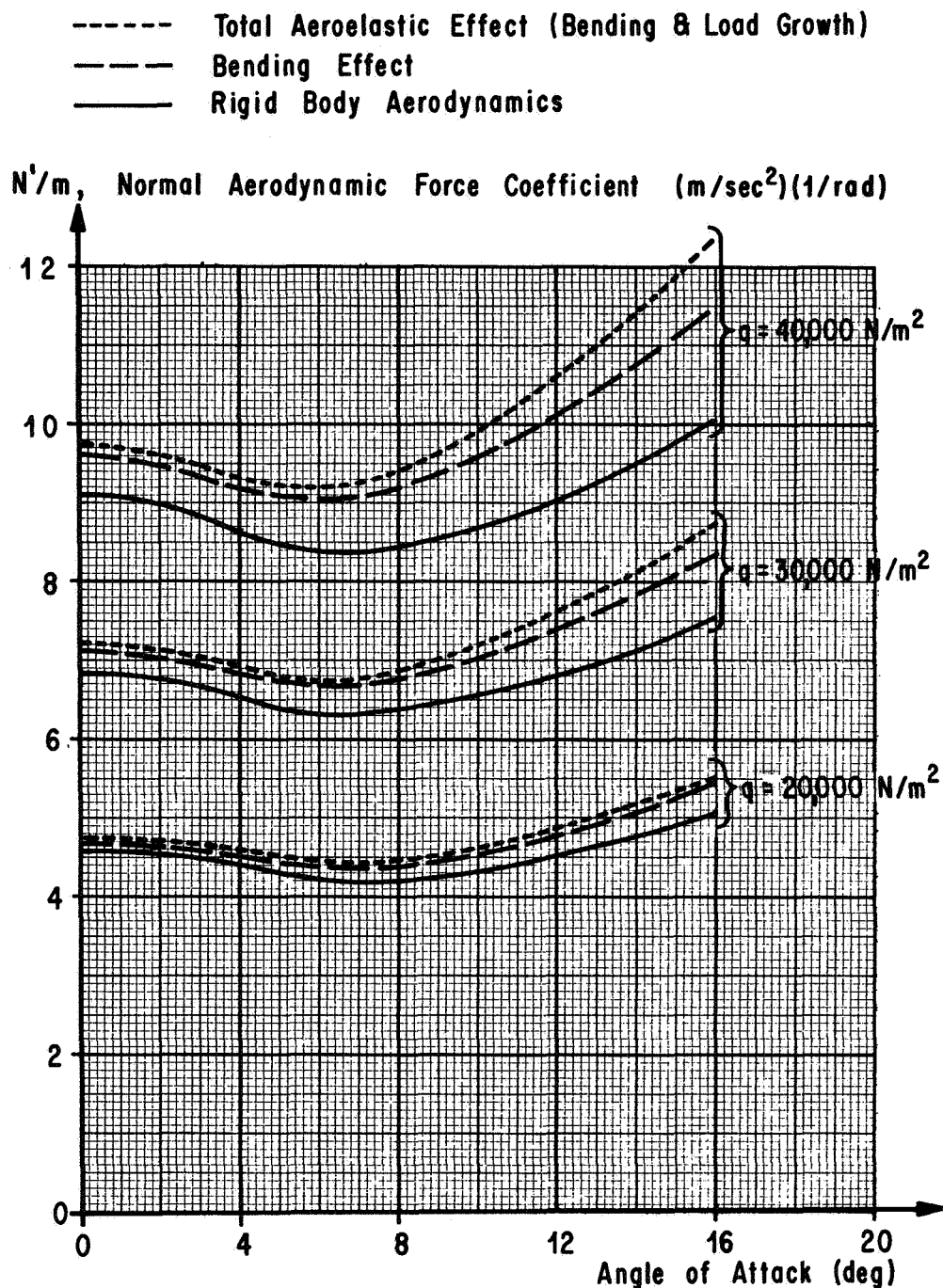FIG. 10. SATURN V AERODYNAMIC BENDING MOMENT INCREASES AT STATION 3100 DUE TO STATIC AEROELASTICITY

Total Aeroelastic Effect (Bending & Load Growth)
Bending Effect
Rigid Body Aerodynamics

N'/m, Normal Aerodynamic Force Coefficient (m/sec²)(1/rad)

FIG. 11. SATURN V INCREASES IN
NORMAL FORCE COEFFICIENT AT MACH 1.2

22

Total Aeroelastic Effect (Bending & Load Growth)
- - - Bending Effect
——— Rigid Body Aerodynamics

C_1, Aerodynamic Moment Coefficient $(rad/sec^2)(1/rad)$

$q = 40000\ N/m^2$

$q = 30000\ N/m^2$

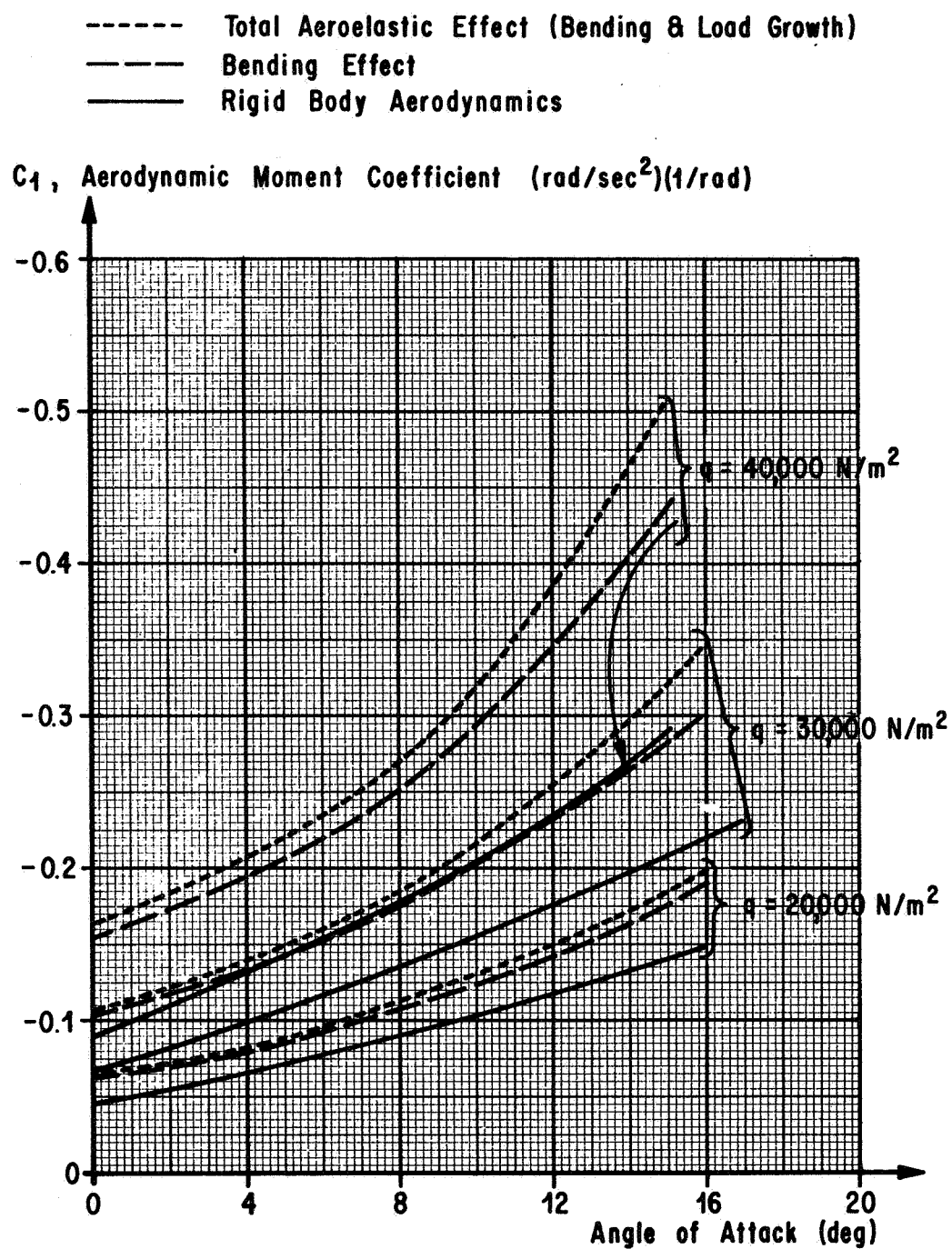$q = 20000\ N/m^2$

Angle of Attack (deg)

FIG. 12. SATURN $\underline{\mathrm{V}}$ INCREASES IN
AERODYNAMIC MOMENT COEFFICIENT AT MACH 1.2

23

FIG. 13. SATURN V INCREASES IN
NORMAL FORCE COEFFICIENT AT MACH 1.7

Total Aeroelastic Effect (Bending & Load Growth)

Bending Effect

Rigid Body Aerodynamics

C_1, Aerodynamic Moment Coefficient $(rad/sec^2)(1/rad)$

$q = 35,000 \ N/m^2$

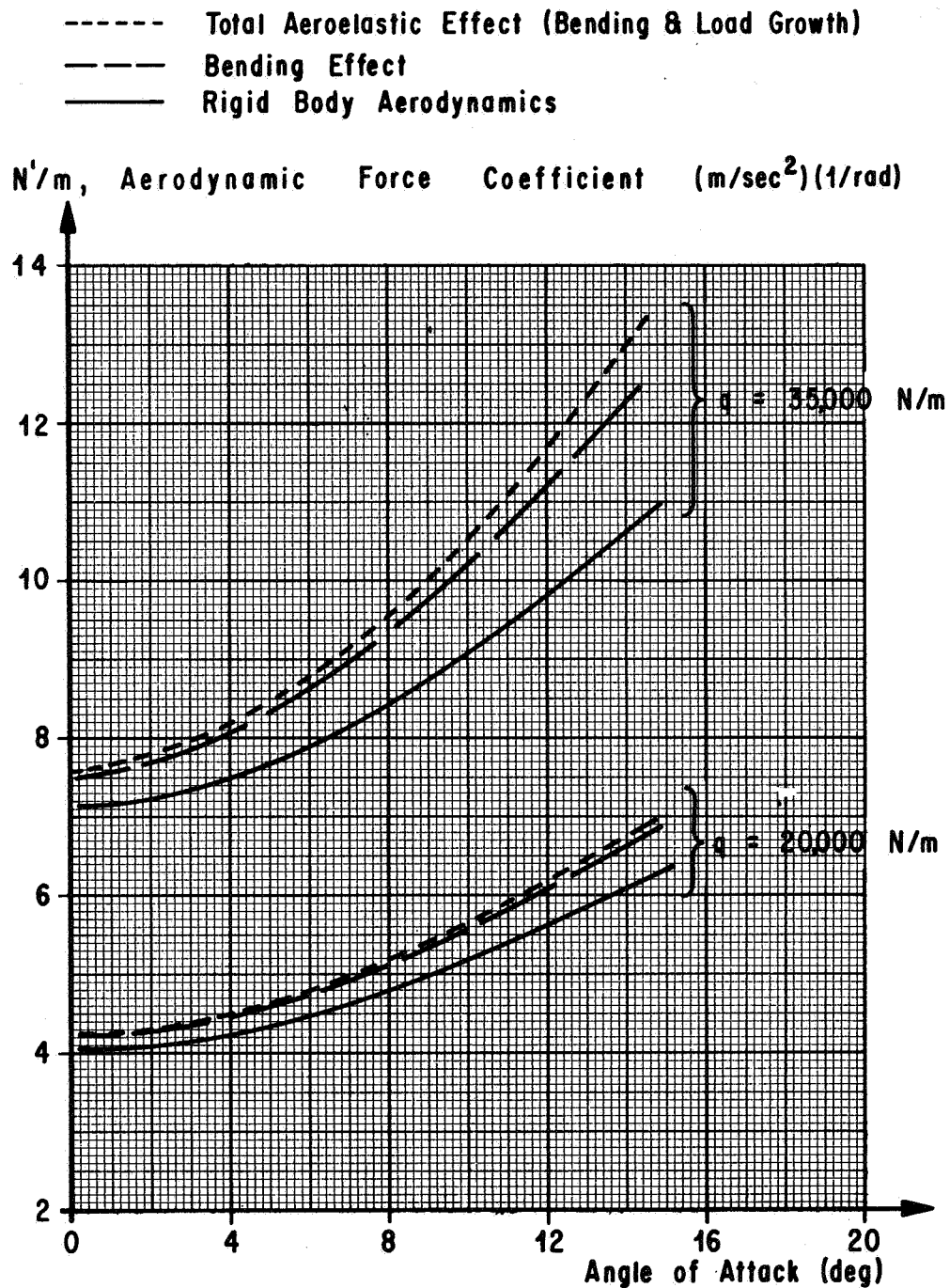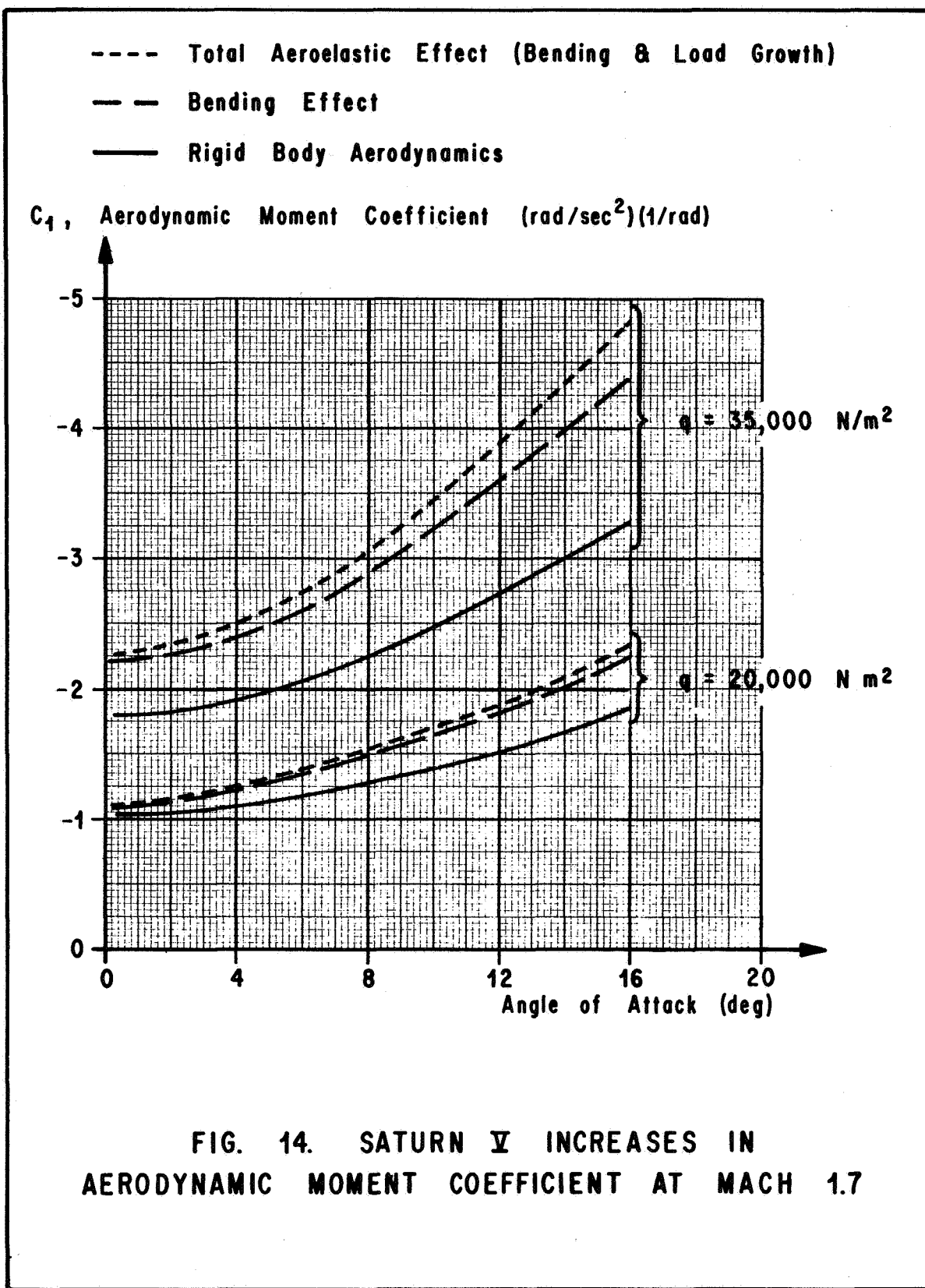$q = 20,000 \ N m^2$

Angle of Attack (deg)

FIG. 14. SATURN V INCREASES IN
AERODYNAMIC MOMENT COEFFICIENT AT MACH 1.7

REFERENCES

1. Papadopoulos, James G., "Aeroelastic Solution for a Wing with A Tip Control Surface," Journal of the Aero/Space Sciences, November 1958.

2. Nunley, Billy W., "The Aerodynamic Characteristics of the Saturn I/Apollo Vehicles (SA-6 and SA-7)," NASA TM X-53056, June 1964.

3. Saturn FEWG, "Results of the Sixth Saturn I Launch Vehicle Test Flight, MPR-SAT-FE-64-16, Confidential.

4. Saturn FEWG, "Results of the Seventh Saturn I Launch Vehicle Test Flight," MPR-SAT-fE-64-17, November 1964, Confidential.

5. Saturn FEWG, "Results of the Ninth Saturn I Launch Vehicle Test Flight SA-8," MPR-SAT-FE-65-11, July 1965, Confidential.

6. Saturn FEWG, "Results of the Eight Saturn I Launch Vehicle Test Flight SA-9," MPR-SAT-FE-65-6, April 1965, Confidential.

7. Nunley, Billy W., "Static Aerodynamic Characteristics of the Apollo-Saturn IB Vehicle," NASA TM X-53348, October 1965.

8. Vehicle Aerodynamic Section, "Static Aerodynamic Characteristics of the Apollo-Saturn V Vehicle," NASA TM X-53517, September 1966.
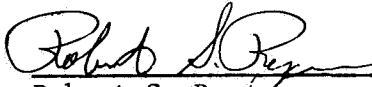
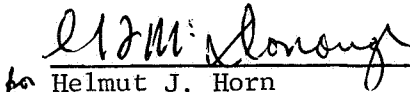AEROELASTIC LOAD GROWTH EFFECTS ON SATURN CONFIGURATIONS

by James G. Papadopoulos

The information in this report has been reviewed for security classification. Review of any information concerning Department of Defense or Atomic Energy Commission programs has been made by the MSFC Security Classification Officer. This report, in its entirety, has been determined to be unclassified.

This document has also been reviewed and approved for technical accuracy.

Robert S. Ryan
Chief, Dynamics Analysis Branch

Helmut J. Horn
Chief, Dynamics and Flight Mechanics Division

E. D. Geissler
Director, Aero-Astrodynamics Laboratory

DISTRIBUTION

DIR

DEP-T

MS-IP

MS-IPL (8)

MS-H

I-RM-M

CC-P

MS-T (6)

R-ASTR
  Dr. Haeussermann
  Mr. Hosenthien
  Mr. B. Moore
  Mr. Blackstone
  Mr. Mink
  Mr. Seltzer
  Mr. Fisher
  Mr. Nicaise

R-P&VE
  Dr. Lucas
  Mr. Hellebrand
  Mr. Goerner
  Mr. Kroll
  Mr. Hunt
  Mr. Furman
  Mr. Paul
  Mr. Wood
  Mr. Platt
  Mr. Swalley

R-COMP
  Dr. Hoelzer
  Mr. Hubbard
  Mr. Scollard
  Mrs. Bryant

Chrysler (MICHOUD)
Attn: Mr. Wells

R-AERO
  Dr. Geissler
  Mr. Jean
  Mr. Horn
  Dr. McDonough
  Mr. Ryan
  Mr. Papadopoulos (25)
  Mr. Townsend
  Mr. Verderaime
  Mr. Bugg
  Mr. Cremin
  Mr. Rheinfurth
  Mrs. Chandler
  Mr. Dahm
  Mr. Linsley
  Mr. Dunn
  Mr. Hensen
  Mr. Lindberg
  Mr. Fulmer
  Mr. Hagood
  Mr. Horst
  Mr. McNiel
  Mr. Weissler
  Mr. Craighead
  Mr. Ernsberger
  Mr. Moore
  Mr. W. Vaughan
  Dr. Scoggins
  Dr. H. Krause
  Dr. Liu
  Mr. Murphree

Scientific and Tech. Info. Facility (25)
P. O. Box 33
College Park, Md.
Attn: NASA Rep. (S-AK/RKT)

Chrysler Corp Space Div.
New Orleans/R. Wells

Boeing
Huntsville, Ala.
Attn: Mr. Haskell
      Mr. Rowe

Lockheed
Huntsville, Ala.
Attn: Mr. Beiber

28